



HAL
open science

New Slope-Normalised Global Gully Density and Orientation Maps for Mars

Susan J. Conway, T. N Harrison, R. J Soare, A. Britton, L. J Steele

► **To cite this version:**

Susan J. Conway, T. N Harrison, R. J Soare, A. Britton, L. J Steele. New Slope-Normalised Global Gully Density and Orientation Maps for Mars. The Geological Society, London, Special Publications, 2019, 467 (1), pp.187-197. 10.1144/SP467.3 . hal-02270628

HAL Id: hal-02270628

<https://hal.science/hal-02270628>

Submitted on 26 Aug 2019

HAL is a multi-disciplinary open access archive for the deposit and dissemination of scientific research documents, whether they are published or not. The documents may come from teaching and research institutions in France or abroad, or from public or private research centers.

L'archive ouverte pluridisciplinaire **HAL**, est destinée au dépôt et à la diffusion de documents scientifiques de niveau recherche, publiés ou non, émanant des établissements d'enseignement et de recherche français ou étrangers, des laboratoires publics ou privés.

1 **New Slope-Normalised Global Gully Density and Orientation Maps for Mars**

2 S. J. Conway^{1,2*}

3 T.N. Harrison^{3,5}

4 R. J. Soare⁴

5 A. Britton^{2,6}

6 L. J. Steele²

7 ¹Laboratoire de Planétologie et Géodynamique de Nantes- UMR CNRS 6112, 2 rue de la
8 Houssinière - BP 92208, 44322 Nantes Cedex 3, France.

9 ²Department of Physical Sciences, Open University, Milton Keynes, MK7 6AA, UK.

10 ³ Centre for Planetary Science and Exploration, University of Western Ontario, London, N6A
11 5B7, Canada.

12 ⁴Department of Geography, Dawson College, 3040 Sherbrooke St. W., Montreal, H3Z 1A4,
13 Canada.

14 ⁵Now at Arizona State University, Tempe, AZ 85287, USA

15 ⁶Now at, Malin Space Science Systems, San Diego, CA 92191, USA

16 *Correspondence to: susan.conway@univ-nantes.fr

17 Running title: New Gully Density and Orientation Maps for Mars

18 **Abstract**

19 We re-analyse the global distribution of gullies in order to provide a set of observational
20 constraints that models of gully formation must explain. We validate our results derived from
21 the global data with four detailed case-studies. We show that the availability of steep slopes is
22 an essential factor to consider when assessing the spatial distribution and abundance of gullies.
23 When availability of steep slopes is taken into account it reveals, with a few exceptions, that
24 gullies are found almost uniformly across the whole 30-90° latitude band. Our analysis also
25 reveals that massive ice deposits are anti-correlated with gullies, and that the undulations in the
26 equatorward limits of the gully distribution could be explained by longitudinal variations in
27 maximum surface temperatures (controlled by variation in surface properties including thermal
28 inertia, and albedo). We find a sharp transition in both hemispheres between pole-facing
29 gullies, which extend from 30° to 40° to a more mixed, but dominantly equator-facing
30 orientation of gullies poleward of 40°. We have no definitive explanation for this transition,
31 but based on previous studies we suggest it could be linked to the availability of near-surface
32 ice deposits.

33 Kilometre-scale gullies are found ubiquitously on steep slopes at the mid-latitudes of
34 Mars (e.g., Balme *et al.*, 2006; Dickson *et al.*, 2007; Heldmann *et al.*, 2005; Kneissl *et al.*,
35 2010). They formed within the last few millions of years (Johnsson *et al.*, 2014; Reiss *et al.*,
36 2004; Schon *et al.*, 2009a) and resemble water-carved gullies on Earth (Malin and Edgett,
37 2000). Martian gullies are defined as features comprised of an alcove, channel and debris apron
38 (Malin and Edgett, 2000) and are found on crater walls, knobs, valley walls and sand dunes
39 (e.g., Balme *et al.*, 2006). The distribution of gullies has a clear latitude dependence: they are
40 very rare and maybe even absent altogether, in the equatorial latitudes between 30°N and 30°S
41 and they are extremely common at latitudes around 35°N and S, with the number of gullies
42 observed dropping off towards the poles (e.g., Dickson *et al.*, 2007). It is known that the
43 frequency of steep slopes generally decreases towards the poles (Kreslavsky *et al.*, 2008;
44 Kreslavsky and Head, 2000), which is thought to be partly due to the presence of a draping
45 deposit that mutes the topographic relief at scales of tens to hundreds of metres. The general
46 decrease of gully density from the mid-latitudes to the poles is thought to be partly explained
47 by the decrease in the number of steep slopes (Dickson *et al.*, 2007). However, this has not
48 been quantitatively assessed. In addition, the orientation of gullies is dependent on latitude: at
49 the mid-latitudes gullies tend to face the pole and at high latitudes they have less preference,
50 but some studies have found an equator-facing preference (Bridges and Lackner, 2006;
51 Heldmann *et al.*, 2007).

52 Together, the latitudinal trends in gully orientation and density suggest an insolation,
53 or climatic, factor is acting in their formation (Costard *et al.*, 2002). However, in order to be
54 able to test different models of gully formation, reliable and precise data are needed on the
55 slope-angle, slope-orientation and latitudinal distribution of gullies.

56 Here we undertake a re-analysis of the global gully dataset recently published by
57 Harrison *et al.* (2015) in order to quantify the effect of slope, orientation and latitude on gully

58 density. We complement this with similar analyses performed on a more detailed dataset in
59 four regions of interest. The second analysis is performed in order to verify the results derived
60 from the global data.

61

62 **Approach**

63 *Global data reanalysis*

64 The global gully dataset compiled by Harrison *et al.* (2015) comprises a series of points placed
65 on features which host gullies. Each point is attributed with a dominant orientation. We perform
66 the following three analyses: gully density, gully density normalized by steep slopes, and a N-
67 S orientation analysis. In all cases we use the standard MOLA 128ppd gridded product, which
68 has a simple cylindrical projection on a spherical Mars datum (radius 3396 km). In order to
69 calculate gully density, we use a 250 km x 250 km moving window and sum the number of
70 gully points in this window for each pixel. We then take account of the distortion of area caused
71 by the map projection, by dividing this by the true area of the moving window, to produce a
72 number of gully points per km² (Fig. 1a). Note that, because of the nature of the original
73 mapping, this method of quantifying gully density does not take into account the density/extent
74 of the gully-features themselves, but rather the features that host them. In some cases this may
75 lead to a single gully being given the same “weight” as an extensive suite of gullies. To generate
76 the slope-normalized gully density, instead of dividing by the true area of the moving window,
77 we divide by the area covered by “steep” pixels in the moving window (Fig. 1b). We define
78 “steep” as being pixels with greater than 20° slope. In order to correct for the influence of the
79 projection in the slope calculation, the fractional slope (S_m) is first calculated in a conformal
80 Mercator projection. These data are then re-projected into the initial simple cylindrical
81 projection and then corrected as follows: $180/\pi \operatorname{atan}(S_m / \cos(L))$, where L is the latitude. The
82 number of pixels with slopes greater than or equal to 20° is then counted per 250 km x 250 km

83 moving window; this count is weighted to take account of the projection, therefore
84 compensating for over-counting towards the pole. Each count is then multiplied by the true
85 area of a pixel for that latitude.

86 Finally, we calculate the ratio between the frequency of pole-facing gullies and the
87 summed frequency of pole- and equator-facing gullies for a 250 km x 250 km moving window
88 in order to better visualize the global trends in gully orientation (Fig. 1c).

89

90 ***Regional site analyses***

91 Gully slopes are mapped as polygons using ArcGIS and the Java Mission-planning and
92 Analysis for Remote Sensing (JMARS) software package (Christensen *et al.*, 2009) (Fig. 2).
93 The base layer is generated principally by using the Mars Reconnaissance Context camera
94 (CTX) images at 6 m/pix. Where there is no CTX coverage, poor CTX image quality or deep
95 shadows on slopes, we use the Mars Express High Resolution Stereo Camera (HRSC) at
96 12.5 m/pix and Mars Odyssey's Thermal Emission Imaging Spectrometer visual images
97 (THEMIS-VIS) at 18 m/pix. The detail of the mapped polygon outlines is simplified to the
98 100 m-scale, because the aim was to sample the underlying Mars Orbiter Laser Altimeter
99 (MOLA) elevation data, which have a grid-spacing of ~463 m.

100 The MOLA data are projected into a Lambert Conformal Conic projection with
101 standard parallels of 34°S/N and 56°S/N and a centre latitude of 45°S/N preserving the pixel
102 size of 463 m. For Terra Cimmeria a central meridian of 154°E is used, 43°W for the two
103 Argyre sites and 15°W for Acidalia Planitia. We split the Argyre region into two sites along
104 the 42.4°E longitude line, to allow us to compare sites with similar spatial extents. We derive
105 slope and aspect from the reprojected MOLA data and then use the polygons to define pixels
106 that contain or do not contain gullies. We considered using the raw MOLA point data to derive
107 slope and aspect. However, erroneous tracks have not been adjusted/removed from this dataset

108 (see discussions in: Neumann *et al.*, 2001; Smith *et al.*, 2001; Som, 2008) and such erroneous
109 tracks cause topographic steps, which are exaggerated in derivative data-products. These
110 discontinuities would be more detrimental to our results than the inclusion of interpolated
111 pixels present in the gridded data. In our Lambert Conformal Conic projection the maximum
112 linear distortion is found at 45° latitude, where it is < 2%, resulting in up to ±0.5° error in slope
113 at slope of 45° and ±0.2° at 10°. This linear distortion results in the real areal extent of a pixel
114 varying by up to 2% of the nominal 214 369 m² value and hence the calculated pixel densities
115 having an uncertainty of the same magnitude.

116

117 **Results**

118 *Gully density*

119 The global gully density map in Fig. 1a reinforces the observations reported in other works,
120 most recently Harrison *et al.* (2015). In brief, gullies begin to be visible poleward of ~30-35°
121 in both hemispheres, with the highest densities being found in the southern hemisphere at
122 ~35°S in Promethei Terra, Terra Sirenum and Terra Cimmeria, at ~45° around the rim of the
123 Argyre Basin and high-latitude outliers at ~70-80°S in the south polar pits (Sisyphi Cavi and
124 Cavi Angusti). For latitudes above 30°, gully density has an inverse relationship with latitude,
125 *i.e.* gully density tends to decline towards the poles. Densities range up to 19 gully sites per
126 100 km² with a mean of 0.64.

127 The global trends noted above are supported by our regional studies. The percentage of
128 pixels occupied by gullies in each of the study sites divided up by latitude is shown in Fig. 3a
129 and has a maximum value of 1.4%. Gullied slopes are concentrated in a band between 30° and
130 55° in the Terra Cimmeria (in the southern hemisphere) and Acidalia Planitia (in the northern
131 hemisphere) sites. In the west Argyre site they are found between 35 and 60°S; by contrast,
132 they are found across a wider latitudinal band from 30°S to 60°S in the east Argyre site. The

133 peak in density in Terra Cimmeria (incidentally coinciding with the Newton Basin) lies in the
134 35-40°S bin and is consistent with the peak in density in the published data from the southern
135 hemisphere study of Heldmann and Mellon (2004). They found that gully density peaked
136 between 33-36°S, where density was measured as the fraction of MOC (Mars Orbiter Camera)
137 narrow-angle (>1.4 m/pix) images containing clear evidence of gullies. However, at the two
138 Argyre sites the peak in gully density lies within the 45-50°S interval, with a particularly large
139 peak in the west Argyre site located in the western Nereidum Montes, the area studied by Raack
140 *et al.* (2012). Here, the highest regional density of gullied slopes is found. Gullies are of
141 universally low density across the Acidalia Planitia site.

142

143 ***Gully density on steep slopes***

144 We know that gullies only occur on slopes, because they are formed by gravitational transport,
145 hence a better comparison of gully density is necessary to consider gully density on only
146 sloping terrain – this is shown for our global data in Fig. 1b and for our regional data in Fig. 3b.

147 Compared to the simple density map in Fig. 1a, the slope-normalized-density-map does
148 not show such clear latitudinally distinct regions of gully concentration. Zones with high
149 density are more evenly scattered across the whole distribution. Gullies tend to be denser
150 towards the higher latitudinal limits of their distribution, rather than the mid-latitudes as
151 suggested by the non-normalized data. Densities on steep slopes range up to 1 million gully
152 sites per 100 km², which is a result of gully sites present in zones with very small areas of steep
153 slopes. The mean density is 940 gully sites per 100 km² of steeply sloping terrain.

154 For our regional sites, when the frequency of gullies per latitude is considered in terms
155 of the percentage of pixels with slope-values $\geq 20^\circ$ occupied by gullies, instead of simple
156 frequency, the sites now have more similar densities to one another, as suggested by the global
157 data. The percent of pixels occupied by gullies now extends up to ~30%. Most notably the

158 Acidalia Planitia site now has similar densities to the other three sites and it is now this site
159 which possesses the overall highest density. The gully density is almost uniformly high
160 between 40°S and 55°S in Terra Cimmeria, with both the Argyre sites having similar densities
161 to Terra Cimmeria in the interval 45-50°S. The West Argyre site no longer has an unusually
162 high density compared to the other sites, but does retain a significant peak associated with the
163 western Nereidum Montes. In the 35-45°S interval in both Argyre sites there is a lower density
164 of slopes with gullies compared to both Terra Cimmeria and the global trends. West Argyre,
165 Terra Cimmeria and Acidalia Planitia have peaks in density in the 45-50° latitude interval. The
166 previously published global trends in gully density no longer match very well with any of our
167 regional datasets (Fig. 3b).

168

169 *Gully orientation*

170 Our global analysis of the ratio of poleward-to-equatorward-facing gully sites agrees in general
171 with previous work (Balme *et al.*, 2006; Dickson *et al.*, 2007; Heldmann and Mellon, 2004;
172 Kneissl *et al.*, 2010), but reveals a sharp transition between pole-facing only gully sites to
173 dominantly equator-facing sites at ~40°. At latitudes equatorward of 40° almost all gully sites
174 have a poleward facing preference, with some exceptions on the northern rim of Hellas and in
175 the northern hemisphere. In contrast, at latitudes poleward of 40° the orientation preference
176 tends to be equatorward, but is more mixed, with notable patches having dominant pole-facing
177 preference. Fig. 3c has been filtered to remove zones with low gully density.

178 Fig. 4 shows gully orientation in our four detailed study regions, for slopes $\geq 10^\circ$ and
179 although these data provide more detail, the overall patterns agree with the global data in
180 Fig. 3c. East Argyre, Terra Cimmeria and Acidalia Planitia follow the global orientation trends;
181 where from 30° to 40° gully sites are oriented towards the pole, 40-45° is a transition zone and
182 at >45° the orientation is predominantly equatorward. West Argyre, also follows this general

183 pattern, but has an additional population of pole-facing gullies at latitudes $>40^{\circ}\text{S}$, which was
184 previously identified by Raack *et al.* (2012).

185 The sparse nature of northern gullies provides an explanation for the conflicting
186 orientation results of previous studies. Bridges and Lackner (2006) found gullies in 72 MOC
187 images (>1.4 m/pix) and 24 THEMIS-VIS images (18 m/pix) and Heldmann *et al.* (2007)
188 found gullies in 137 MOC images and both studies reported an equator-facing orientation
189 preference at all latitudes. However, Kneissl *et al.* (2010) found a transition from pole-facing
190 at 30° - 40°N to equator-facing at 30° - 40°N with contradictory results $>50^{\circ}\text{N}$ using MOC and
191 HRSC images (12.5 m/pix). *et al. et al.* From our new analysis it is clear that orientation trends
192 are only clearly visible where there are dense populations of gullies, a criterion which was not
193 used in the previous studies, hence these new density maps are particularly useful where gullies
194 are sparse in the northern mid-latitudes.

195

196 **Discussion**

197 *Reconsidering factors influencing the global gully density*

198 Our analyses show that in general the latitudinal distribution of gullies, poleward of 40° , is
199 well-explained by the availability of steep slopes – a relation cited by previous work (*e.g.*,
200 Dickson *et al.*, 2007), but not quantified. Further, our analyses reveal that there are places in
201 this latitudinal zone with steep slopes yet no gullies, or a low density of gullies. In the northern
202 hemisphere, these zones coincide with the scarps of the polar cap, individual impact craters,
203 and Phlegra Montes. In the southern hemisphere these zones coincide with scarps of the polar
204 cap, a few individual impact craters, Promethei and Thyles Rupes, and a zone to the east of
205 Hellas in Promethei Terra. The polar cap scarps are comprised almost pure ice sculpted by
206 wind (Howard, 2000) and hence are not expected to host gullies. The scarps associated with
207 Promethei and Thyles Rupes could be very short hillslopes which therefore might host gullies

208 not detectable at the CTX resolution of the Harrison *et al.* (2015) survey. In Fig. 5a we plot the
209 distribution of Lobate Debris Aprons (LDA) collated by van Gasselt (2007) and of Glacier Like
210 Forms (GLF) from Souness *et al.* (2012) along with our global gully density and slope-
211 distribution data, and it can be seen that in the vast majority of areas with LDA and GLF have
212 either low gully density or have no mapped gullies. Therefore, the presence of LDA/GLF could
213 explain the relative paucity of gullies in Nereidum Montes, Promethei Terra, Phlegra Montes,
214 Erebus Montes and in Deutero-Protonilus Mensae noted above.

215 LDA are features where the presence of thick (tens to hundreds of meters) ice has been
216 confirmed in certain examples through analysis of radar data (Holt *et al.*, 2008; Plaut *et al.*,
217 2009). The present day morphology of LDA and GLF is indicative of relict debris-covered ice
218 (*e.g.*, Arfstrom and Hartmann, 2005; Head *et al.*, 2010; Hubbard *et al.*, 2011; Squyres and Carr,
219 1986) and these comprise the most substantial ice deposits outside the polar areas (Levy *et al.*,
220 2014). The presence of substantial ice in the subsurface will increase the thermal inertia of the
221 surface, which could inhibit gully-formation mechanisms related to ice-thaw, or CO₂
222 sublimation. Alternately the morphology of the terrain associated with the presence of LDA
223 and GLF could be inhibiting gully-formation. Another possibility is that such features could
224 cover-up gullies (de Haas *et al.*, 2017). Gullies are known to occur in close association with
225 arcuate ridges (interpreted to be end-moraines; Arfstrom and Hartmann, 2005; Berman *et al.*,
226 2005; Head *et al.*, 2008) and other signs of degraded “glaciers” (Dickson *et al.*, 2015). Hence,
227 the interrelation between these two features appears to be complex. In any case, this is a new
228 factor that should be taken into account when assessing mechanisms of gully-formation.

229 Although we do not show the distribution of Concentric Crater Fill (CCF), which are
230 infilled craters also believed to contain extant ice under a lag cover (*e.g.*, Levy *et al.*, 2010;
231 Squyres and Carr, 1986), their distribution covers almost uniformly the whole 30-50° N and S
232 latitude bands (Dickson *et al.*, 2012; Levy *et al.*, 2010). Therefore, conversely to LDA/GLF

233 their distribution does not seem to affect the distribution of gullies. CCF does not generally
234 extend up onto the walls of the host craters, thus we might not expect an influence on gully-
235 distribution. Because CCF infills the crater it reduces the total length of the crater-wall (but
236 likely not its slope), so we might expect a reduction of the length of the gullies in such craters.
237 Some of the individual craters without gullies at latitudes $>60^\circ$ in both hemispheres are those
238 filled with mounds of polar-cap-like deposits (Conway *et al.*, 2012; Westbrook, 2009). For
239 other individual craters we found no obvious reason that could explain the lack of gullies.

240 The undulations in the lower latitude boundary of the gully distribution at around
241 $30\text{-}35^\circ\text{N/S}$ is not caused by a lack of steep slopes (Fig. 5a), or by the presence of massive ice
242 deposits. As suggested in previous work this boundary could be imposed by the ability to
243 emplace, or to melt surface ice deposits under previous high obliquity climate excursions
244 (Costard *et al.*, 2002; Madeleine *et al.*, 2014). Fig. 5b shows that for any given latitude gullies
245 tend to be present where the annual day mean surface temperature is the highest for that
246 latitude, under current orbital and climate conditions, suggesting ability to melt/sublimate
247 might be the dominant factor, rather than ability to deposit ice. We emphasize that the
248 correlation is not perfect, there are gullies found in “cold spots” on the Tharsis bulge and in
249 Promethei Terra. Additionally we have used surface temperature data derived from a GCM
250 where present data orbital and atmospheric parameters were used. This simulation included the
251 assimilation of Mars Climate Sounder temperature profiles and dust optical depths. The
252 assimilation procedure allows us to obtain the best possible representation of the present-day
253 climate. Full details of the GCM and assimilation procedure can be found in Lewis *et al.* (2007)
254 and Steele *et al.* (2014).. However, we feel that it is reasonable to expect that the longitudinal
255 variations in maximum daily average surface temperature should not vary significantly with
256 changes in orbital parameters, providing the surface properties are similar. This is because for
257 a given latitude, the longitudinal temperature variation is mostly driven by changes in the

258 albedo and thermal inertia of the regolith (e.g., Mellon and Jakosky, 1993). Areas with the
259 highest mean daily surface temperatures tend to have low albedo and high thermal inertia (and
260 vice versa for the areas with the lowest mean daily surface temperatures). Detailed climate
261 model runs are beyond the scope of this work, but should be performed in the future to verify
262 this apparent correlation.

263

264 ***Orientation***

265 The latitudinal distribution of gullies overlaps with that of the “Latitude Dependent Mantle”
266 (LDM): a surface-draping deposit thought to comprise an airfall deposit of ice and dust
267 (Kreslavsky and Head, 2002; Mustard *et al.*, 2001). At the mid-latitudes where gullies are most
268 common, the LDM exhibits signs of degradation (pitting, erosional scarps) and becomes more
269 intact with increasing latitude (Milliken *et al.*, 2003; Mustard *et al.*, 2001). The same climatic
270 arguments have been raised to explain the increasing degradation of the LDM towards the
271 equator (e.g., Mustard *et al.*, 2001), as to explain the latitude dependent distribution of gullies.
272 This had led some researchers to link gullies with degradation of the LDM (Bridges and
273 Lackner, 2006; Dickson *et al.*, 2015; Levy *et al.*, 2011; Raack *et al.*, 2012; Schon and Head,
274 2012). Although no systematic mapping has been performed to ascertain the orientation of the
275 slopes hosting LDM, in the 30-40° latitude range where pole-facing gullies are observed,
276 Vincendon *et al.* (2010) noted that the geographical distribution of seasonal CO₂ frost indicated
277 subsurface water-ice must be present on pole-facing slopes in this latitude range. Dickson *et*
278 *al.* (2015) suggest that the LDM provides an erodible substrate, allowing gully channels to be
279 expressed, therefore the fact that the LDM is generally found on pole-facing slopes in the 30-
280 40° latitude range, could explain the predominantly pole-facing gully orientations.

281 However, it is worth noting here that the degraded terrain-muting unit mapped by
282 Mustard *et al.* (2001) and referred to in many other papers (Kostama *et al.*, 2006; Kreslavsky

283 and Head, 2002, 2000; Milliken *et al.*, 2003; Schon *et al.*, 2009b), may not be the same unit as
284 the deposit which hosts the gullies, originally called “pasted-on terrain” by Christensen (2003),
285 but often named LDM in subsequent publications (Conway and Balme, 2014; Dickson *et al.*,
286 2015; Dickson and Head, 2009; Levy *et al.*, 2011, 2009). Conway and Balme (2014) noted the
287 polygonally patterned and often ribbed unit into which gullies incise is substantially thicker
288 (up to 30 m) than the LDM measured on the plains (around several metres; Kreslavsky and
289 Head, 2002; Mustard *et al.*, 2001; Schon *et al.*, 2009b). Soare *et al.* (2017) have also noted that
290 the polygonally-patterned unit into which gullies incise is located stratigraphically below the
291 LDM found on the inter-crater plains and exhibits a different suite of degradation features from
292 the LDM. This “pasted-on” unit could be related to the mid-latitude crater asymmetry noted by
293 Conway and Mangold (2013), or incipient formation of glacier-like-forms (e.g., Head *et al.*,
294 2008). In addition, many gully systems do not originate in areas covered in “LDM” (Aston *et al.*,
295 *et al.*, 2011) and there are also examples of gullies present where no evidence for “LDM” is found
296 at all (Johnsson *et al.* 2014, de Haas *et al.*, 2015a, 2015b).

297

298 **Conclusions**

299 We conclude that the availability of steep slopes must be taken into account to perform a fair
300 assessment of global gully density.

301 From these analyses we conclude that any model of gully formation would have to explain the
302 following:

- 303 • The onset of gully forming processes at $\sim 30^\circ$ N/S and the undulations in that boundary.
- 304 • The generally uniform gully forming potential in the whole $30\text{-}55^\circ$ latitude band.
- 305 • Local paucity of gullies (e.g. Promethei Terra), which appear to coincide with massive
306 ice deposits.

- 307 • The sharp transition from almost uniquely pole-facing to dominantly equator-facing,
308 being consistently located at $\sim 40^\circ\text{N/S}$.

309

310 **Acknowledgements**

311 We thank Ginny Gulick and one anonymous reviewer for their helpful comments with which
312 we improved the manuscript. SJC acknowledges funding from the Leverhulme Trust in support
313 of this work (grant number RPG-397) and support from the French Space Agency, CNES.

314 **8. References cited:**

- 315 Arfstrom, J., Hartmann, W.K., 2005. Martian flow features, moraine-like ridges, and gullies:
316 Terrestrial analogs and interrelationships. *Icarus* 174, 321–335.
- 317 Aston, A.H., Conway, S.J., Balme, M.R., 2011. Identifying Martian gully evolution. *Geol. Soc. Lond.*
318 *Spec. Publ.* 356, 151–169. doi:10.1144/SP356.9
- 319 Balme, M., Mangold, N., Baratoux, D., Costard, F., Gosselin, M., Masson, P., Pinet, P., Neukum, G.,
320 2006. Orientation and distribution of recent gullies in the southern hemisphere of Mars:
321 Observations from High Resolution Stereo Camera/Mars Express (HRSC/MEX) and Mars
322 Orbiter Camera/Mars Global Surveyor (MOC/MGS) data. *J. Geophys. Res. Planets* 111,
323 doi:10.1029/2005JE002607.
- 324 Berman, D.C., Hartmann, W.K., Crown, D.A., Baker, V.R., 2005. The role of arcuate ridges and gullies
325 in the degradation of craters in the Newton Basin region of Mars. *Icarus* 178, 465–486.
- 326 Bridges, N.T., Lackner, C.N., 2006. Northern hemisphere Martian gullies and mantled terrain:
327 Implications for near-surface water migration in Mars' recent past. *J. Geophys. Res. Planets*
328 111, 09014. doi:10.1029/2006JE002702
- 329 Christensen, P.R., 2003. Formation of recent martian gullies through melting of extensive water-rich
330 snow deposits. *Nature* 422, 45–48.
- 331 Christensen, P.R., Engle, E., Anwar, S., Dickenshied, S., Noss, D., Gorelick, N., Weiss-Malik, M., 2009.
332 JMARS-A Planetary GIS, in: AGU Fall Meeting Abstracts. p. 06.
- 333 Conway, S.J., Balme, M.R., 2014. Decametre-thick remnant glacial ice deposits on Mars. *Geophys.*
334 *Res. Lett.* 41, 5402–5409. doi:10.1002/2014GL060314
- 335 Conway, S.J., Hovius, N., Barnie, T., Besserer, J., Le Mouélic, S., Orosei, R., Read, N.A., 2012. Climate-
336 driven deposition of water ice and the formation of mounds in craters in Mars' north polar
337 region. *Icarus* 220, 174–193. doi:10.1016/j.icarus.2012.04.021
- 338 Conway, S.J., Mangold, N., 2013. Evidence for Amazonian mid-latitude glaciation on Mars from
339 impact crater asymmetry. *Icarus* 225, 413–423. doi:10.1016/j.icarus.2013.04.013

340 Costard, F., Forget, F., Mangold, N., Peulvast, J.P., 2002. Formation of recent Martian debris flows by
341 melting of near-surface ground ice at high obliquity. *Science* 295, 110–113.
342 doi:10.1126/science.1066698

343 de Haas, T., Conway, S.J., Butcher, F.E.G., Levy, J.S., Grindrod, P.M., Balme, M.R., Goudge, T.A., 2017.
344 Time will tell: temporal evolution of Martian gullies and paleoclimatic implications. *Geol.*
345 *Soc. Lond. Spec. Publ.* this volume, in review.

346 de Haas, T., Conway, S.J., Krautblatter, M., 2015a. Recent (Late Amazonian) enhanced
347 backweathering rates on Mars: Paracratering evidence from gully alcoves: LATE AMAZONIAN
348 BACKWEATHERING RATES. *J. Geophys. Res. Planets* 120, 2169–2189.
349 doi:10.1002/2015JE004915

350 de Haas, T., Hauber, E., Conway, S.J., van Steijn, H., Johnsson, A., Kleinhans, M.G., 2015b. Earth-like
351 aqueous debris-flow activity on Mars at high orbital obliquity in the last million years. *Nat.*
352 *Commun.* 6. doi:10.1038/ncomms8543

353 Dickson, J.L., Head, J.W., 2009. The formation and evolution of youthful gullies on Mars: Gullies as
354 the late-stage phase of Mars' most recent ice age. *Icarus* 204, 63–86.

355 Dickson, J.L., Head, J.W., Fassett, C.I., 2012. Patterns of accumulation and flow of ice in the mid-
356 latitudes of Mars during the Amazonian. *Icarus* 219, 723–732.
357 doi:10.1016/j.icarus.2012.03.010

358 Dickson, J.L., Head, J.W., Goudge, T.A., Barbieri, L., 2015. Recent climate cycles on Mars:
359 Stratigraphic relationships between multiple generations of gullies and the latitude
360 dependent mantle. *Icarus* 252, 83–94. doi:10.1016/j.icarus.2014.12.035

361 Dickson, J.L., Head, J.W., Kreslavsky, M., 2007. Martian gullies in the southern mid-latitudes of Mars:
362 Evidence for climate-controlled formation of young fluvial features based upon local and
363 global topography. *Icarus* 188, 315–323.

364 Harrison, T.N., Osinski, G.R., Tornabene, L.L., Jones, E., 2015. Global Documentation of Gullies with
365 the Mars Reconnaissance Orbiter Context Camera and Implications for Their Formation.
366 *Icarus* 252, 236–254. doi:10.1016/j.icarus.2015.01.022

367 Head, J.W., Marchant, D.R., Dickson, J.L., Kress, A.M., Baker, D.M., 2010. Northern mid-latitude
368 glaciation in the Late Amazonian period of Mars: Criteria for the recognition of debris-
369 covered glacier and valley glacier landsystem deposits. *Earth Planet. Sci. Lett.* 294, 306–320.
370 doi:DOI: 10.1016/j.epsl.2009.06.041

371 Head, J.W., Marchant, D.R., Kreslavsky, M.A., 2008. Formation of gullies on Mars: Link to recent
372 climate history and insolation microenvironments implicate surface water flow origin. *Proc.*
373 *Natl. Acad. Sci. U. S. A.* 105, 13258–13263.

374 Heldmann, J.L., Carlsson, E., Johansson, H., Mellon, M.T., Toon, O.B., 2007. Observations of martian
375 gullies and constraints on potential formation mechanisms II. The northern hemisphere.
376 *Icarus* 188, 324–344.

377 Heldmann, J.L., Mellon, M.T., 2004. Observations of martian gullies and constraints on potential
378 formation mechanisms. *Icarus* 168, 285–304.

379 Heldmann, J.L., Toon, O.B., Pollard, W.H., Mellon, M.T., Pitlick, J., McKay, C.P., Andersen, D.T., 2005.
380 Formation of Martian gullies by the action of liquid water flowing under current Martian
381 environmental conditions. *J Geophys Res-Planets* 110, doi:10.1029/2004JE002261.

382 Holt, J.W., Safaeinili, A., Plaut, J.J., Head, J.W., Phillips, R.J., Seu, R., Kempf, S.D., Choudhary, P.,
383 Young, D.A., Putzig, N.E., Biccari, D., Gim, Y., 2008. Radar Sounding Evidence for Buried
384 Glaciers in the Southern Mid-Latitudes of Mars. *Science* 322, 1235–1238.

385 Howard, A. D. (2000). The role of eolian processes in forming surface features of the Martian polar
386 layered deposits. *Icarus*, 144(2), 267-288.

387 Hubbard, B., Milliken, R.E., Kargel, J.S., Limaye, A., Souness, C., 2011. Geomorphological
388 characterisation and interpretation of a mid-latitude glacier-like form: Hellas Planitia, Mars.
389 *Icarus* 211, 330–346. doi:10.1016/j.icarus.2010.10.021

390 Johnsson, A., Reiss, D., Hauber, E., Hiesinger, H., Zanetti, M., 2014. Evidence for very recent melt-
391 water and debris flow activity in gullies in a young mid-latitude crater on Mars. *Icarus* 235,
392 37–54. doi:10.1016/j.icarus.2014.03.005

393 Kneissl, T., Reiss, D., van Gasselt, S., Neukum, G., 2010. Distribution and orientation of northern-
394 hemisphere gullies on Mars from the evaluation of HRSC and MOC-NA data. *Earth Planet.*
395 *Sci. Lett.* 294, 357–367. doi:j.epsl.2009.05.018

396 Kostama, V.-P., Kreslavsky, M.A., Head, J.W., 2006. Recent high-latitude icy mantle in the northern
397 plains of Mars: Characteristics and ages of emplacement. *Geophys Res Lett* 33, L11201.
398 doi:10.1029/2006GL025946

399 Kreslavsky, M.A., Head, J.W., 2002. Mars: Nature and evolution of young latitude-dependent water-
400 ice-rich mantle. *Geophys. Res. Lett.* 29, 14–1. doi:10.1029/2002GL015392

401 Kreslavsky, M.A., Head, J.W., 2000. Kilometer-scale roughness of Mars: Results from MOLA data
402 analysis. *J. Geophys. Res.* 105, 26695–26712. doi:10.1029/2000JE001259

403 Kreslavsky, M.A., Head, J.W., Marchant, D.R., 2008. Periods of active permafrost layer formation
404 during the geological history of Mars: Implications for circum-polar and mid-latitude surface
405 processes. *Planet. Space Sci.* 56, 289–302. doi:10.1016/j.pss.2006.02.010

406 Levy, J., Head, J.W., Marchant, D.R., 2010. Concentric crater fill in the northern mid-latitudes of
407 Mars: Formation processes and relationships to similar landforms of glacial origin. *Icarus*
408 209, 390–404. doi:10.1016/j.icarus.2010.03.036

409 Levy, J.S., Fassett, C.I., Head, J.W., Schwartz, C., Watters, J.L., 2014. Sequestered glacial ice
410 contribution to the global Martian water budget: Geometric constraints on the volume of
411 remnant, midlatitude debris-covered glaciers. *J. Geophys. Res. Planets* 119, 2014JE004685.
412 doi:10.1002/2014JE004685

413 Levy, J.S., Head, J.W., Marchant, D.R., 2011. Gullies, polygons and mantles in Martian permafrost
414 environments: cold desert landforms and sedimentary processes during recent Martian
415 geological history. *Geol. Soc. Lond. Spec. Publ.* 354, 167–182. doi:10.1144/SP354.10

416 Levy, J.S., Head, J.W., Marchant, D.R., Dickson, J.L., Morgan, G.A., 2009. Geologically recent gully-
417 polygon relationships on Mars: Insights from the Antarctic dry valleys on the roles of
418 permafrost, microclimates, and water sources for surface flow. *Icarus* 201, 113–126.

419 Lewis, S. R., Read, P. L., Conrath, B. J., Pearl, J. C., Smith, M. D., 2007. Assimilation of Thermal
420 Emission Spectrometer atmospheric data during the Mars Global Surveyor aerobraking
421 period. *Icarus* 192, 327–347.

422 Madeleine, J.-B., Head, J.W., Forget, F., Navarro, T., Millour, E., Spiga, A., Colaïtis, A., Määttänen, A.,
423 Montmessin, F., Dickson, J.L., 2014. Recent Ice Ages on Mars: The role of radiatively active
424 clouds and cloud microphysics. *Geophys. Res. Lett.* n/a-n/a. doi:10.1002/2014GL059861

425 Malin, M.C., Edgett, K.S., 2000. Evidence for recent groundwater seepage and surface runoff on
426 Mars. *Science* 288, 2330–2335. doi:10.1126/science.288.5475.2330

427 Mellon, M.T., Jakosky, B.M., 1993. Geographic variations in the thermal and diffusive stability of
428 ground ice on Mars. *J. Geophys. Res.* 98, 3345. doi:10.1029/92JE02355

429 Milliken, R.E., Mustard, J.F., Goldsby, D.L., 2003. Viscous flow features on the surface of Mars:
430 Observations from high-resolution Mars Orbiter Camera (MOC) images. *J Geophys Res* 108,
431 doi:10.1029/2002JE002005.

432 Mustard, J.F., Cooper, C.D., Rifkin, M.K., 2001. Evidence for recent climate change on Mars from the
433 identification of youthful near-surface ground ice. *Nature* 412, 411–414.
434 doi:10.1038/35086515

435 Neumann, G.A., Rowlands, D.D., Lemoine, F.G., Smith, D.E., Zuber, M.T., 2001. Crossover analysis of
436 Mars Orbiter Laser Altimeter data. *J. Geophys. Res. Planets* 106, 23753–23768.
437 doi:10.1029/2000JE001381

438 Plaut, J.J., Safaeinili, A., Holt, J.W., Phillips, R.J., Head, J.W., Seu, R., Putzig, N.E., Frigeri, A., 2009.
439 Radar evidence for ice in lobate debris aprons in the mid-northern latitudes of Mars.
440 *Geophys. Res. Lett.* 36, 02203.

441 Raack, J., Reiss, D., Hiesinger, H., 2012. Gullies and their relationships to the dust-ice mantle in the
442 northwestern Argyre Basin, Mars. *Icarus* 219, 129–141. doi:10.1016/j.icarus.2012.02.025

443 Reiss, D., van Gasselt, S., Neukum, G., Jaumann, R., 2004. Absolute dune ages and implications for
444 the time of formation of gullies in Nirgal Vallis, Mars. *J Geophys Res-Planets* 109,
445 doi:10.1029/2004JE002251.

446 Schon, S.C., Head, J.W., 2012. Gasa impact crater, Mars: Very young gullies formed from impact into
447 latitude-dependent mantle and debris-covered glacier deposits? *Icarus* 218, 459–477.
448 doi:10.1016/j.icarus.2012.01.002

449 Schon, S.C., Head, J.W., Fassett, C.I., 2009a. Unique chronostratigraphic marker in depositional fan
450 stratigraphy on Mars: Evidence for ca. 1.25 Ma gully activity and surficial meltwater origin.
451 *Geology* 37, 207–210. doi:10.1130/g25398a.1

452 Schon, S.C., Head, J.W., Milliken, R.E., 2009b. A recent ice age on Mars: Evidence for climate
453 oscillations from regional layering in mid-latitude mantling deposits. *Geophys Res Lett* 36,
454 doi:10.1029/2009GL038554. doi:10.1029/2009GL038554

455 Smith, D.E., Zuber, M.T., Frey, H.V., Garvin, J.B., Head, J.W., Muhleman, D.O., Pettengill, G.H.,
456 Phillips, R.J., Solomon, S.C., Zwally, H.J., Banerdt, W.B., Duxbury, T.C., Golombek, M.P.,
457 Lemoine, F.G., Neumann, G.A., Rowlands, D.D., Aharonson, O., Ford, P.G., Ivanov, A.B.,
458 Johnson, C.L., McGovern, P.J., Abshire, J.B., Afzal, R.S., Sun, X., 2001. Mars Orbiter Laser
459 Altimeter: Experiment summary after the first year of global mapping of Mars. *J. Geophys.*
460 *Res. Planets* 106, 23689–23722. doi:10.1029/2000JE001364

461 Soare, R.J., Conway, S.J., Gallagher, C., Dohm, J.M., 2017. Ice-rich (periglacial) vs icy (glacial)
462 depressions in the Argyre region, Mars: a proposed cold-climate dichotomy of landforms.
463 *Icarus* 282, 70–83. doi:10.1016/j.icarus.2016.09.009

464 Som, 2008. The Mars Orbiter Laser Altimeter dataset: Limitations and improvements. *Mars J.* 4, 14–
465 26. doi:10.1555/mars.2008.0002

466 Souness, C., Hubbard, B., Milliken, R.E., Quincey, D., 2012. An inventory and population-scale
467 analysis of Martian glacier-like forms. *Icarus* 217, 243–255. doi:10.1016/j.icarus.2011.10.020
468 Squyres, S.W., Carr, M.H., 1986. Geomorphic Evidence for the Distribution of Ground Ice on Mars.
469 *Science* 231, 249–252. doi:10.1126/science.231.4735.249
470 Steele, L. J., Lewis, S. R., Patel, M. R., 2014. The radiative impact of water ice clouds from a reanalysis
471 of Mars Climate Sounder data. *Geophys. Res. Lett.* 41, 4471–4478.
472 van Gasselt, S., 2007. Cold-Climate Landforms on Mars. der Freien Universität Berlin, Berlin.
473 Vincendon, M., Mustard, J., Forget, F., Kreslavsky, M., Spiga, A., Murchie, S., Bibring, J.-P., 2010.
474 Near-tropical subsurface ice on Mars. *Geophys. Res. Lett.* 37, doi:10.1029/2009GL041426.
475 doi:10.1029/2009gl041426
476 Westbrook, O.W., 2009. Crater ice deposits near the south pole of Mars (Masters). Massachusetts
477 Institute of Technology, Cambridge, MA.

478 **Figure Captions**

479

480 **Figure 1:** Maps derived from re-analysis of the Harrison *et al.* (2015) gully database and the
481 global MOLA topography data. A) Point-density of gullies in number sites per 100 km². B)
482 Point-density of gullies in number sites per 100 km² of steeply sloping terrain, where “steep”
483 is defined as $\geq 20^\circ$. This representation gives an unbiased view of the distribution of gullies
484 and should be used in preference to A). C) The ratio between the frequency of pole-facing
485 gullies and the summed frequency of pole- and equator-facing gullies, where 1= 100% pole-
486 facing and 0 = 100% equator-facing. Pink outlines are the four sites studied in greater detail,
487 EA = East Argyre, WA = West Argyre, TC = Terra Cimmeria and AP = Acidalia Planitia.

488

489 **Figure 2:** Digitisation of gullies as polygons. CTX image P14_006572_1367_XN_43S051W,
490 with colour-coded MOLA topography in the background and digitised gullies as pink
491 outlines. The black and white box in the top-left shows the size of a MOLA pixel for
492 illustration.

493

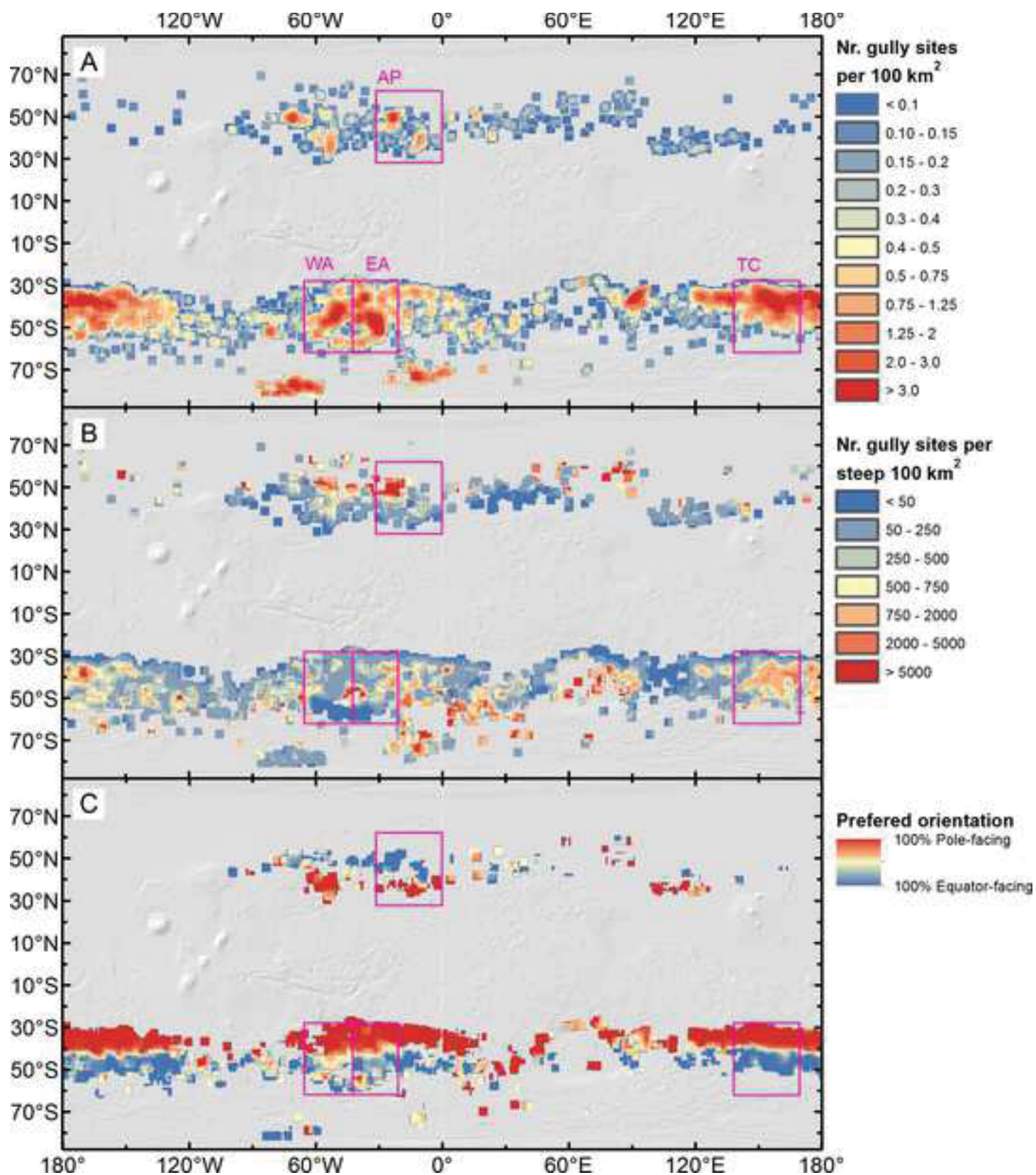
494 **Figure 3:** Top: Percent of pixels with gullies per latitude bin per region. Bottom: Percent of
495 gully occupation on pixels with slopes $> 20^\circ$, per latitude bin, per region. Map projected data
496 were used to calculate the number of pixels, hence the real areal extent could be $\pm 2\%$ the
497 value represented by these bars (and therefore is too small to be visually represented). The
498 grey line is the normalized southern-hemisphere frequency of gullies taken from Dickson and
499 Head (2009), based on data by Heldmann and Mellon (2004), who calculated the percentage
500 of Mars Orbiter Camera images with gullies per 3° latitude bin.

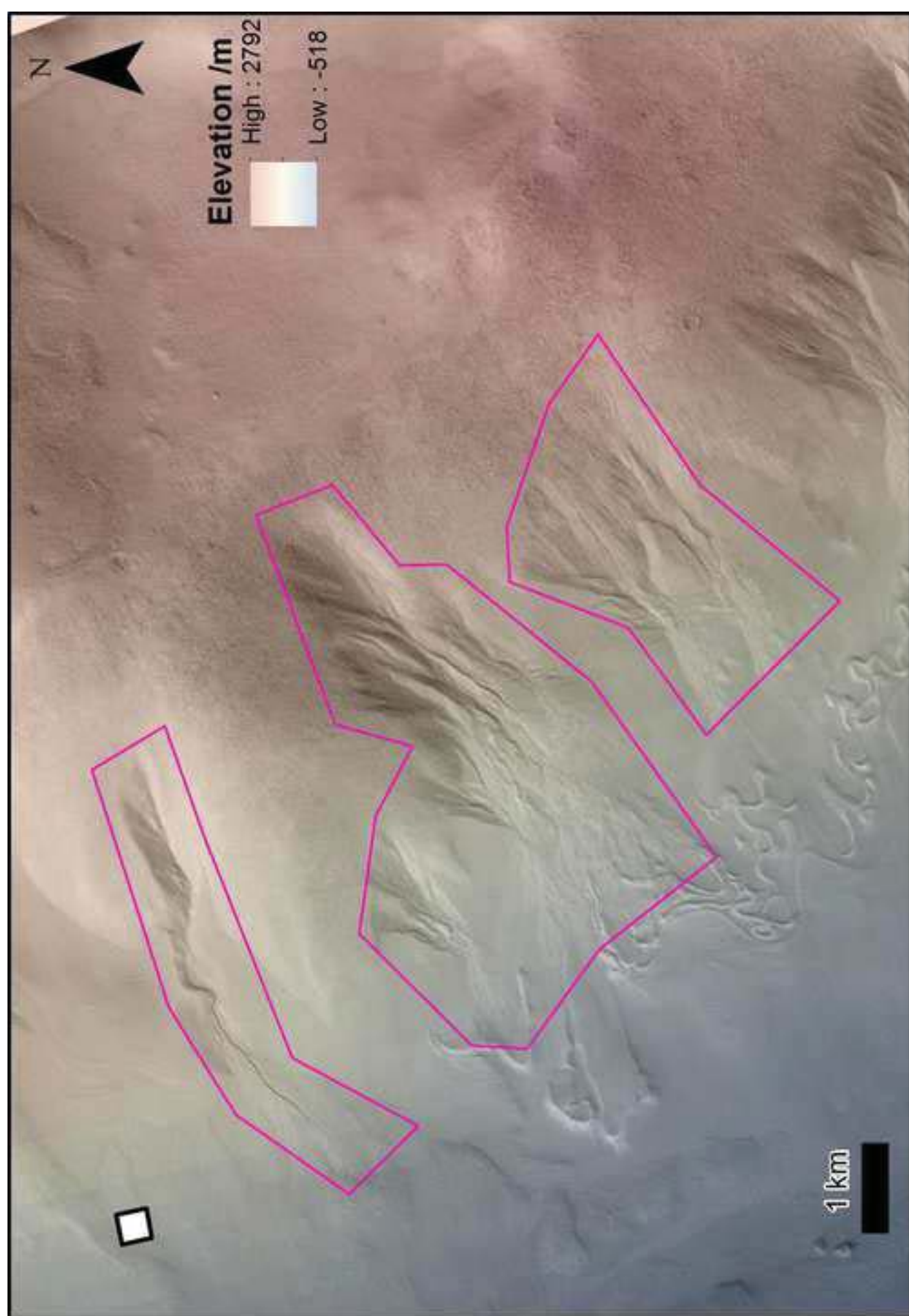
501

502 **Figure 4:** Orientation (aspect) of MOLA pixels containing gullies, per latitude, for the four
503 detailed study sites. Red numbers indicate the value of the outer-ring on the polar-axis, which
504 is the relative frequency of gullies on slopes $> 10^\circ$ for any given orientation in that latitude
505 bin (we used a 10° threshold in this case, otherwise the number of samples per orientation
506 was too small). Therefore gully density ranges between 2.5 and 25%. Note: the northern
507 hemisphere site Acidalia Planum has been mirrored across the x-axis, so that pole-facing
508 slopes are oriented down-page, for ease of comparison with the southern hemisphere sites.

509

510 **Figure 5:** Exploration of variables that may explain the global gully distribution. A) Slopes,
511 LDA, GLF and gullies. Masked out in white are areas with few steep slopes (i.e. $<$
512 15,000,000 “steep” slopes per km^2). B) A map of the year-maximum day-average surface
513 temperature, derived using a similar methodology to Kreslavsky *et al.* (2008), where the
514 temperatures have been re-scaled, so that 1 = maximum temperature for each latitude and 0
515 = minimum temperature for each latitude.





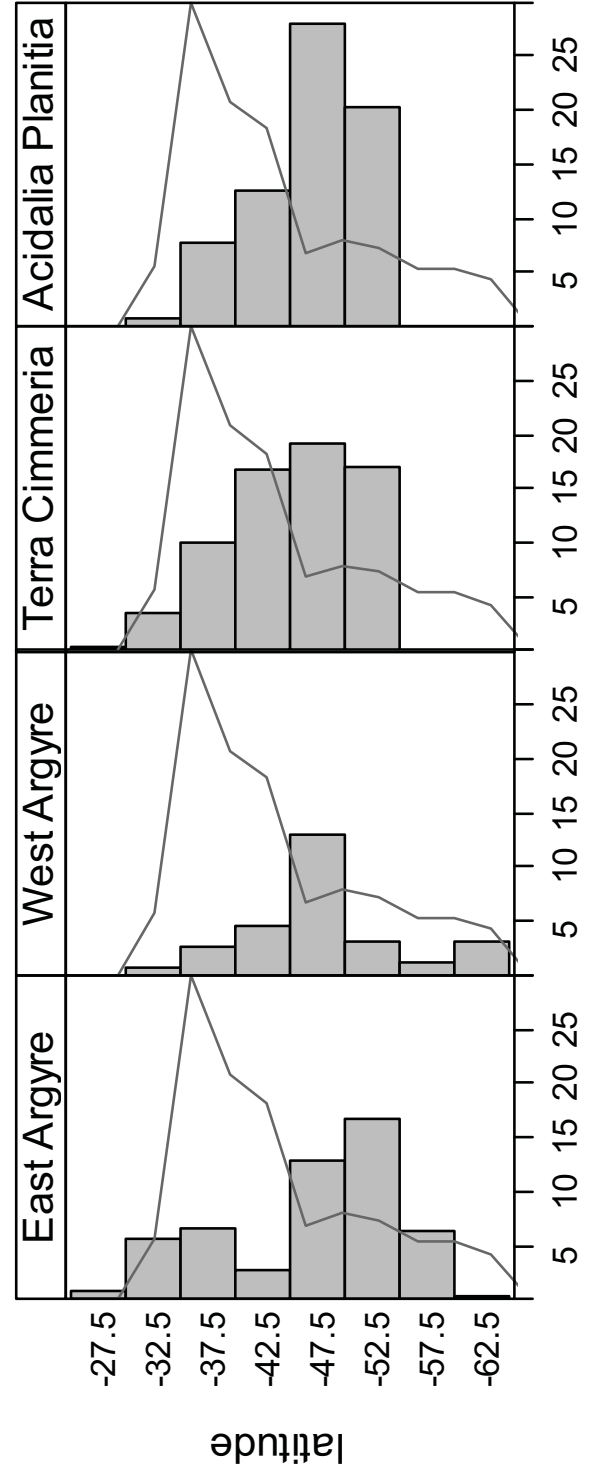
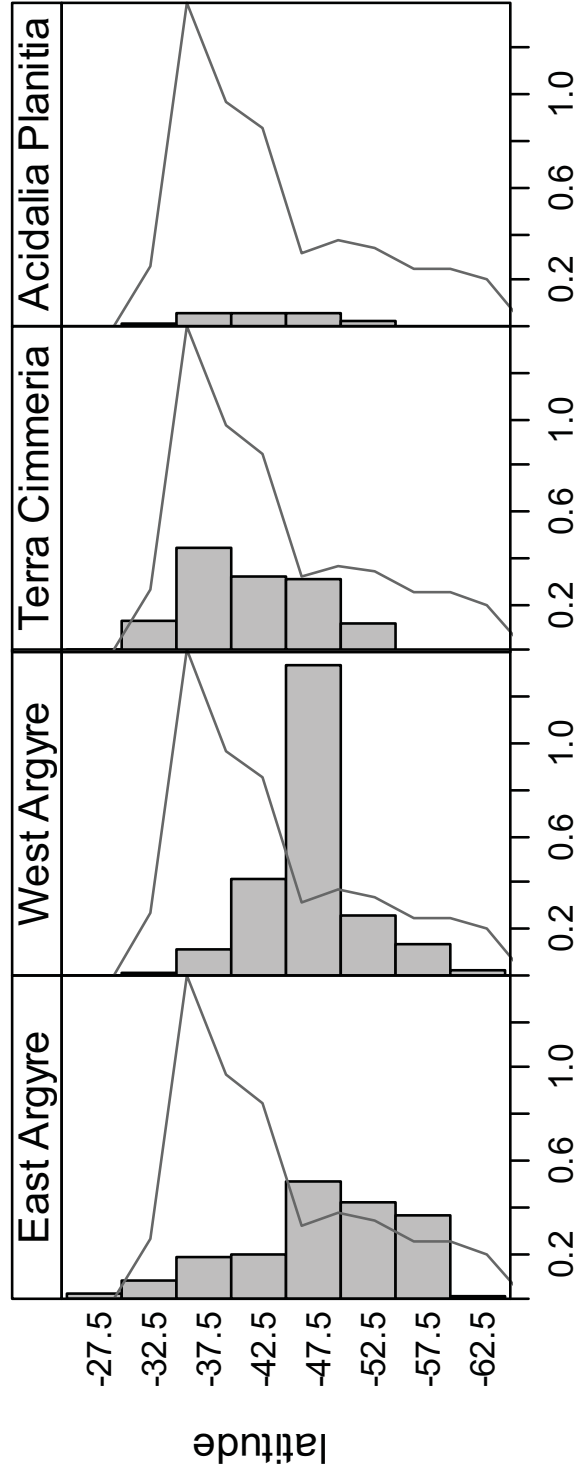


Figure 4

[Click here to download Figure Conway_GSL_Fig4_localOrientation.eps](#)

